# BISTATIC SYNTHETIC APERTURE RADAR TECHNOLOGY - TOPOLOGIES AND APPLICATIONS

Andon Dimitrov Lazarov
*CITS, Bourgas Free University,62 San Stefano Str. Bourgas, Bulgaria*
*lazarov@bfu.bg*

Keywords: Bistatic Synthetic Aperture Radar, Bistatic Forwar Scattering Inverse Synthetic Aperture Radar .

Abstract: Bistatic Synthetic Aperture Radar (BSAR) and Bistatic Forward Inverse Synthetic Aperture Radar (BFISAR) concepts are considered. Different BSAR topologies with transmitter of opportunity, stationary receiver with moving target are analyzed. Forward scattering RCS is defined. Mathematical models of BSAR and BFISAR signals and image reconstruction algorithms are presented. Results of numerical experiment are discussed.

## 1 INTRODUCTION

Bistatic synthetic aperture radar (BSAR) technique is under intensive research activities over the last ten years. It makes an impact on the progress in synthetic aperture radar (SAR) and inverse synthetic aperture radar (ISAR) technologies and meets strong requirements for the further enhancement of microwave remote sensing systems. It is expected that the implementation of BSAR concept in ISAR will enlarge the area of application and improve substantially the functionality of imaging radars.
Bistatic concept in SAR for Earth observation is analyzed in (Moccia A., 2002). Prospective and problems in space-surface BSAR are addressed in (Cherniakov M., 2002) and BSAR with application to moving target detection is described in (Whitewood A., 2003). Several BSAR techniques for image reconstruction have been proposed that provide effective tools for radar imaging of cooperative targets (D'Aria D., 2004). Effects of bistatic configurations on ISAR imaging have been largely investigated in (Martorella M., 2007).

## 2 BISTATIC SYNTHETIC APERTURE RADAR CONFIGURATIONS

### 2.1 Bistatic Radar Geometry

Bistatic radar geometry comprises a transmitter, located in point *A*, a receiver located in point *B*, and target located in point *T* (Fig. 1). Denote θ as a bistatic angle, $L = AB$ as a baseline, and $\Delta_R$ as range resolution

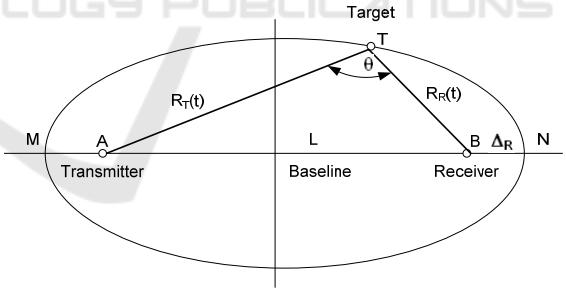


Figure 1: Bistatic radar geometry

Contours of constant bistatic range are ellipses with transmitter and receiver as two foci. The following equations can be written

$$R_T(t) + R_R(t) = L + n.\Delta_R, \quad (1)$$

$$\cos\theta = \frac{R_T^2(t) + R_R^2(t) - L^2}{2R_T(t)R_T(t)}, \quad (2)$$

where $n$ = 0,1,2, ….is the number of an isorange ellipse. The number $n$ = 0 corresponds to zero range resolution on baseline $L$.

Lazarov A.
BISTATIC SYNTHETIC APERTURE RADAR TECHNOLOGY TOPOLOGIES AND APPLICATIONS.
DOI: 10.5220/0005413100030013
In *Proceedings of the First International Conference on Telecommunications and Remote Sensing (ICTRS 2012)*, pages 3-13
ISBN: 978-989-8565-28-0
Copyright © 2012 by SCITEPRESS – Science and Technology Publications, Lda. All rights reserved

## 2.2 Bistatic Radar Equation

Bistatic radar equation represents signal-to-noise ratio as a function of parameters of electromagnetic propagation, radar and target, i.e.

$$\frac{P_R}{P_N} = \frac{P_T G_T G_R F_T^2 F_R^2 \lambda^2 \sigma_B L_p}{(4\pi)^3 R_T^2 R_R^2 k T_0 B F}. \quad (3)$$

where $P_R$ - receiver power; $P_N$ - noise power; $R_T$ - distance from the transmitter to the target; $R_R$ - distance from the receiver to the target $\sigma_B$ - bistatic radar cross − section of the target; $G_T$ - transmitter gain; $G_R$-receiver gain; $F_T^2$ -pattern propagation factor for the transmitter-to-target-path; $F_R^2$ - pattern propagation factor for the target-to-receiver path; $k$ - Boltzmann's constant; $\lambda$ -wavelength; F – Figure of merit; $T_0$ -noise temperature.
The constant detection range is defined by $R_T R_R = \text{const}$ that describes ovals of Cassini around transmitter and receiver points (Fig. 2).

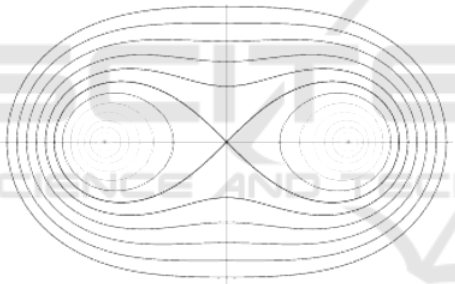

Figure 2: Ovals of Cassini

## 2.3 BSAR for Local Area Monitoring

A new topology of BSAR with non cooperative transmitter is presented in (Cherniakov M., 2009,). The topology includes Global Navigation Satellite Systems (GNSS) as transmitters of opportunity and a stationary receiver placed on the ground. It is a system for local area monitoring. BSAR with non cooperative transmitter is a sub-class class of bistatic SAR systems that comprises a spaceborne transmitter, and a receiver located on or near the Earth's surface (Fig. 3). As a sub-class of BSAR, it encompasses a variety of system topologies. Any communication or Global Positioning System (GPS) satellite can be used as a noncooperative transmitter while the receiver could be airborne, onboard a ground moving vehicle or stationary on the ground.

Different BSAR configurations have been considered (Whitewood A., 2007). It has been the investigated passive BSAR, with GNSS as transmitters of opportunity (such as GPS, GLONASS and Galileo) and an airborne receiver (Antoniou M., 2009).

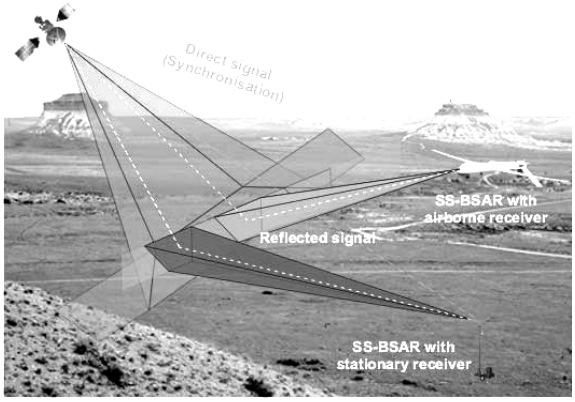


Figure 3: BSAR topologies

An image with a Galileo satellite as a transmitter and a ground moving vehicle as a receiver has been obtained (Fig. 4)

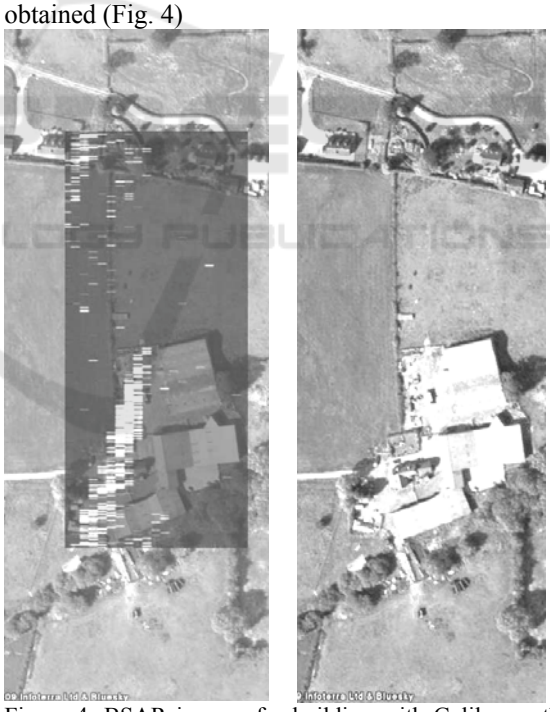

Figure 4: BSAR image of a building with Galileo as the transmitter and a moving ground vehicle as the receiver superimposed on a satellite optical photograph (a), optical photograph (b).

The BSAR topology with a satellite transmitter has military applications based on the potential of the system to operate covertly due to its passive nature, its ability to provide constant monitoring of any

remote region on the Earth due to the global coverage of the GNSS satellites. It is important to investigate whether this system can be implemented, to consider satellite availability, to identify whether fast update rates for change detection can be achieved, to examine basic radar functionality, which involves calculations on integration time, resolution and power budget.

### 2.3.1 Satellite availability and observation time

Satellite availability can help define the available observation time for imaging and the update rates for change detection. It means the number of satellites simultaneously visible at any point in the world and the position of each satellite with respect to the receiver to be defined. An optimal satellite can be used for imaging to minimize degradation in the system's range resolution due to the large bistatic angle (Willis N.J., 2007). It was found that approximately 6-8 satellites are simultaneously visible at a particular point on the Earth, at any time (Zuo R., 2007). Another issue is the achievable observation time. This is defined as the amount of time that a target on the Earth is within the beam of a satellite (assuming it is always within the beam of the receiver). Even though the beam of the GNSS satellites covers a large part of the Earth's surface, the observation time may vary significantly from one satellite to another because of their position with respect to the target. Fig. 5 shows results of Keplerian modelling to define observation time versus satellite number (Cherniakov M., 2009).

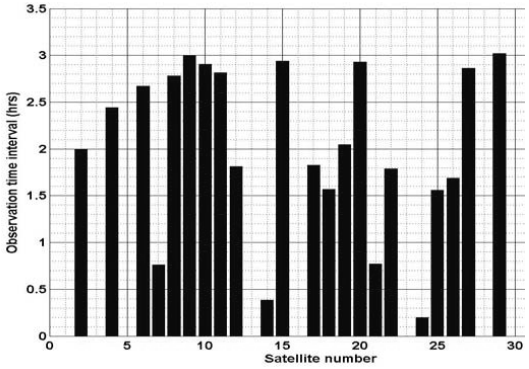


Figure 5: Observation time versus satellite number according to Keplerian modeling

The figure shows that within an interval of one day, 22 satellites are visible in a nearly quasi-monostatic mode, with observation times varying from 12 minutes to 3 hours. These values allow for very long integration times due to satellites' wide beam. It provides fine azimuth resolutions, and enhances power budget of the system.

### 2.3.2 Azimuth resolution

GNSS satellites on MEO with ranges of 23000 km from the Earth, orbital speeds 4 km/s, and long observation time provide a significant improvement in azimuth resolution. The maximum azimuth resolution that can be achieved for data in Fig. 5 is shown in Fig. 6. The resolution is calculated through Doppler bandwidth of the associated GPS azimuth signals, and dividing with the average speed of the satellite towards the observed target. The figure shows that extremely high azimuth resolutions can be potentially achieved if the full observation time is processed. Even for an observation time of 12 minutes the resolution is reasonable.

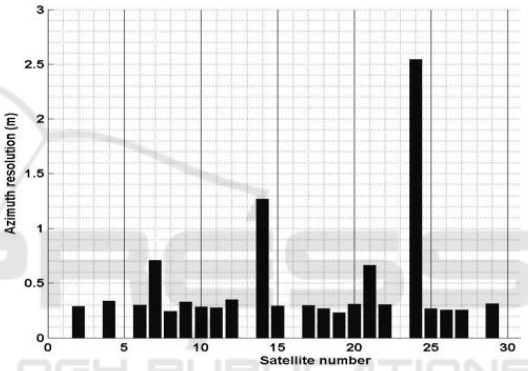


Figure 6: Potential azimuth resolution for SS-BSAR with stationary receiver.

### 2.3.3 Power Budget

Since GNSS satellites exhibit a low signal power density on the Earth's surface, long observation times will essentially enhance the signal-to-noise ratio (SNR) at the output of the image formation algorithm used. Assuming full target signal compression in both range and azimuth, the SNR can be derived as

$$SNR = \frac{P_D G_R \lambda^2 \sigma}{(4\pi)^2 R_R^2 k T_s} T_{\text{int}} \frac{T_{obs}}{\Delta u} \qquad (4)$$

where $P_D$ is the signal power density of the GNSS satellites on the Earth, $G_R$ is the gain of the receiving antenna, $\lambda$ is the radar wavelength, $\sigma$ is the target radar cross section, $R_R$ is the receiver-to-target range, $k$ is Boltzmann's constant, $T_S$ is the receiver noise temperature, $T_{\text{int}}$ is the integration time in the range direction (equal to the length of the transmitted

GNSS code sequence), $T_{obs}$ is the observation time and $\Delta u$ is the azimuth sample spacing.
The challenge in this task is the long integration time, over which the trajectory of the satellite can no longer be considered a straight line. It can be seen in Fig. 7, where the trajectory of one of the satellites in our previous example (Fig. 5, satellite number 14) has been plotted in 3-D space.

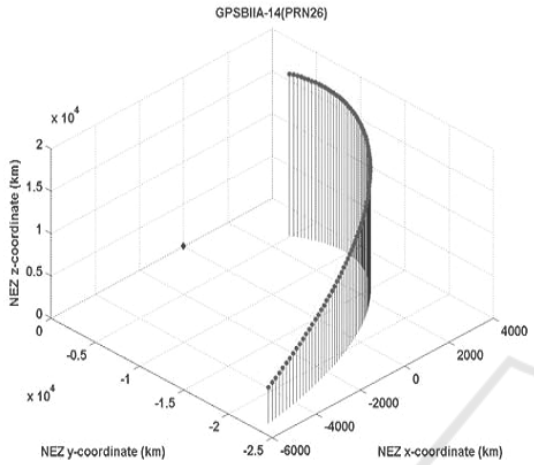


Figure 7: Example of a satellite trajectory over a long observation time (satellite number 14)

### 2.3.4 Signal synchronization in BSAR based on GLONASS satellite emission

BSAR coherent signal processing requires synchronization between the transmitter and the receiver (Fig. 8) (R.Saini, 2009).

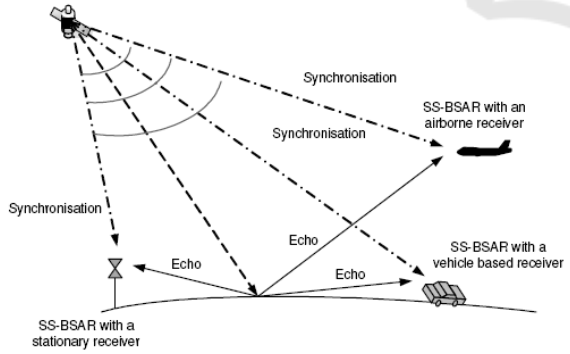


Figure 8: BSAR topolody with synchronization.

Fig. 9 illustrates block diagram of the structure of GLONASS signals transmitted in the $L_1$ frequency band. The C/A and P-code signals are in phase quadrature. The C/A code rate is 511 KHz and the code period is 1 msec. The C/A code sequence is added (mod 2) to a 100 Hz navigation message. The P-code has a chip rate of 5.11 MHz and is a truncated M-sequence repeated every 1 sec. The navigation message on the P-code has a clock rate of 50 Hz. The P-code is used for the purpose of imaging, as it provides a reasonable range resolution of about 30m (quasi-bistatic case) and is no longer encrypted. It is worth mentioning that utilization of a GALILEO satellite $E_5$ signal (20-50 MHz bandwidth) would improve the range resolution to about 3-8 m.

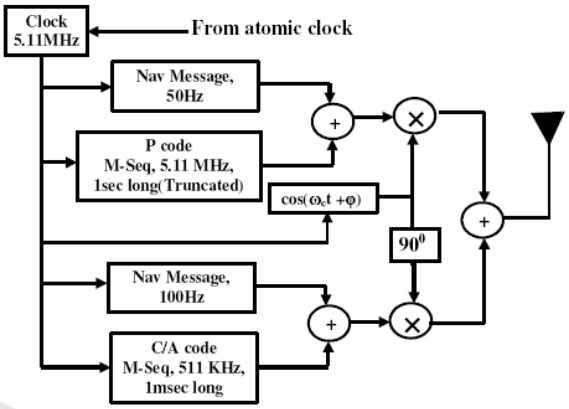


Figure 9: Signal structure of GLONASS

Usually in a radar signal processor, the range compression consists of a correlation of the radar channel signal with the heterodyne channel signal delayed for each range resolution cell in the multi-channel correlator (Fig. 10).

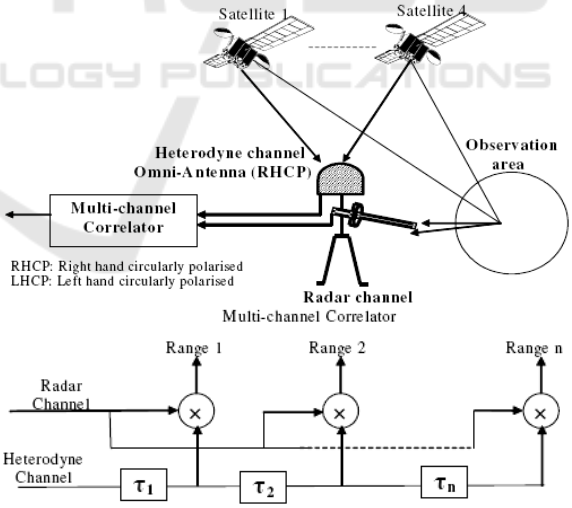


Figure 10: Heterodyne channel with omny antenna (*a*) and multi-channel correlator (*b*).

It was demonstrated that for GLONASS signal it is not possible to directly correlate the heterodyne channel with the radar channel. The signal received from the GLONASS satellite is a superposition of the C/A code and P-code signals, the spectra of which overlap; the P-code (5.11 MHz bandwidth) is used for the purpose of imaging. If the heterodyne

channel is directly correlated with the radar channel, the P-code will be masked by the C/A code at the output of the correlator. The bandwidth of the C/A code is only one-tenth that of the P-code but even if the C/A code of the desired satellite signal is filtered out in the heterodyne channel, the signal correlation properties are degraded by the C/A codes of interfering satellites. It was demonstrated that, if the radar channel signal is correlated with a locally generated signal containing only the P-code, the effect of the C/A code could be suppressed. However this technique needs navigation message decoding which, in turn, requires P-code synchronization. Fig. 11 illustrates a range compression algorithm. Fig. 12 shows a simplified synchronization block diagram.

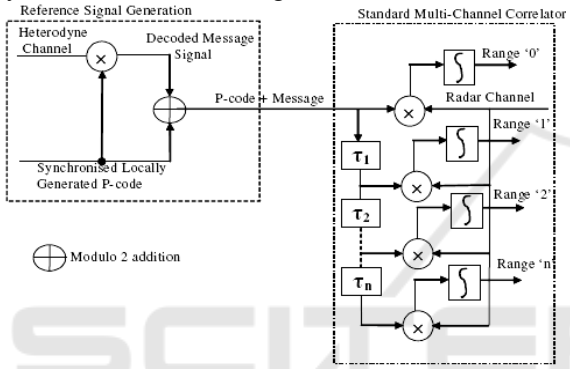


Figure 11: Range compression algorithm.

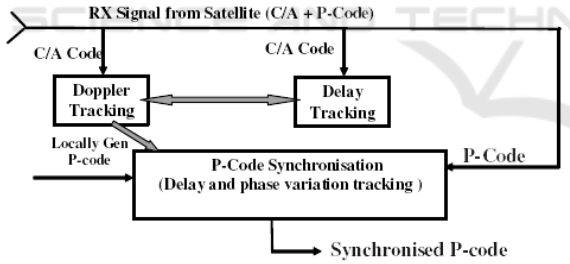


Figure 12: Synchronization block diagram

A synchronization block diagram is presented in Fig. 12. The P-code has a better delay tracking accuracy due to its wider signal bandwidth compared to the C/A code. The synchronization algorithm is based on a conventional delay locked loop, and consists of:
- Doppler extraction using the C/A code and applying conventional phase locked loops.
- Removing the frequency shift from the received P-code by extracting frequency variation.
- Synchronize the locally generated P-code to the Doppler-stripped P-code.
- Decode the navigation message signal by synchronized P-code, fraction of a chip. Once the incoming P-code has been acquired, tracking, or fine synchronization, takes place.

## 2.4 Bistatic generalized inverse synthetic aperture radar

Consider geometry of BSAR scenario with a moving target illuminated by GPS waveform and a stationary GPS receiver. It refers to geometry of Generalized Inverse Synthetic Aperture Radar (GISAR) and Bistatic Synthetic Aperture Radar (BSAR) and regards as Bistatic Generalized Inverse Synthetic Aperture Radar (BGISAR). The problem posed is to describe the discrete geometry of BGISAR scenario and based on it to derive a mathematical model of a BGISAR signal (Lazarov A., 2011).

### 2.4.1 BGISAR Scenario

BGISAR scenario is illustrated in Fig. 13 where GPS transmitter, receiver (located on the land surface) and a target are all situated in *Oxyz*, where $\mathbf{R}^{S}(p)$ is the current position vector of the transmitter in discrete time instant *p*, $\mathbf{R}_{00'}(p)$ is the current position vector of the mass center of the target, $\mathbf{R}^{r}$ is the stationary position vector of the receiver. The target presented as an assembly of point scatterers is depicted in Cartesian coordinate system *OXYZ*, where $\mathbf{R}_{ijk}$ is the position vector of the *ijk*th point scatterer.

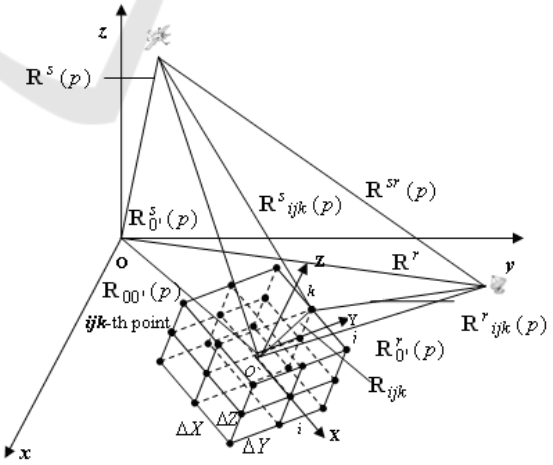


Figure 13: BGISAR geometry

In Fig. 13: $\mathbf{R}^{S}_{0'}(p)$ - the position vector of the target's mass center with respect to the transmitter, $\mathbf{R}^{r}_{0'}(p)$ - The position vector of the target's mass

center with respect to the receiver, $\mathbf{R}^{s}_{ijk}(p)$ - the position vector of the *ijk*th point scatterer with respect to the transmitter, $\mathbf{R}^{s}_{ijk}(p)$ - the position vector of the *ijk*th point scatterer with respect to the receive, $\Delta X$, $\Delta Y$, $\Delta Z$ – dimensions of the resolution cell.

The round trip distance from GPS transmitter to the target and GPS receiver is defined by

$$R_{ijk}(p) = \left|\mathbf{R}^{s}{}_{ijk}(p)\right| + \left|\mathbf{R}^{r}{}_{ijk}(p)\right|. \quad (5)$$

The deterministic component of the BGISAR signal, reflected by all point scatterers of the object for every $p$ th GPS C/A pulse train has the form

$$S(p,t) = \sum_{ijk} a_{ijk}\mathbf{rect}[T_{ijk}(p)]\mathbf{exp}\begin{Bmatrix} -j[\omega(t-t_{ijk}(p))] \\ +\pi b(t)] \end{Bmatrix} \quad (6)$$

where $T_{ijk}(p) = \dfrac{t - t_{ijk}(p)}{T}$ is the time parameter

$\omega = 2\pi c/\lambda$ is the angular frequency, $c = 3.10^{8}$ m/s is the velocity of the light, $b(t)$ is the binary parameter of the C/A phase code modulated pulse train, defined by coefficients of two Gold polynomials, $a_{ijk}$ is the reflective coefficient of the *ijk*th point scatterer, three-dimensional (3-D) image function; $T$ is the time duration of the C/A phase code, $t_{ijk}(p) = \dfrac{R_{ijk}(p)}{c}$ is the round trip delay to $ijk$ th point scatterer; $t = t_{ijk\,\min}(p) + (k-1)\Delta T$, $\Delta T$ is the time duration of the phase segment, $k$ is the current number of segment, $K = T/\Delta T = 1023$ is the full number of segments of the C/A phase code, is the relative dimension of the target.

The image extraction procedure comprises

1. Phase correction, $\tilde{S}(p,k) = \hat{S}(p,k).\mathbf{exp}(j\Phi(p))$,

2. Range compression by cross-correlation,

$$\tilde{S}(\hat{p},\hat{k}) = \sum_{k=\hat{k}}^{\hat{k}+K-1} \tilde{S}(p,k)\mathbf{exp}[j\pi b((k-\hat{k}+1)\Delta T)],$$

3. Azimuth compression by Fourier transform,

$$a_{ijk}(\hat{p},\hat{k}) = \sum_{p=\overline{1,N}} \tilde{S}(p,\hat{k})\mathbf{exp}\left\{ j\left[\frac{2\pi}{N}\hat{p}p\right]\right\}.$$

### 2.4.2 BGISAR numerical experiment

A numerical experiment was carried out to verify the geometry and 3-D model of BGISAR signal with GPS C/A code phase modulation and to prove the correctness of developed digital signal image reconstruction procedure. It is assumed that the target, a flying helicopter is moving rectilinearly in a 3-D Cartesian coordinate system of observation $Oxyz$. GPS transmitter emits a C/A code train. GPS satellite velocity: $v = 3819{,}206$ m/s. Coordinates of the stationary GPS receiver: $x^{r} = 55$ m, $y^{r} = 45$ m and $z^{r} = 30$ m. The trajectory parameters of the target: velocity $V = 80$ m/s; guiding angles. Parameters of the GPS C/A pulse trains: wavelength $\lambda = 19{,}1.10^{-2}$ m (carrier frequency $f = 1.57.10^{9}$ Hz), registration time interval $T_{p} = 2{,}2.10^{-3}$ s, GPS C/A code PRF 1.023 MHz and respective time duration of the segment of the C/A pulse $\Delta T = 0.9775.10^{-6}$ s, time duration of GPS C/A code $T = 10^{-3}$ s; full number of GPS C/A pulses $K = 1023$, number of transmitted GPS C/A code trains during aperture synthesis $N = 1024$. In Fig. 2 results are presented.

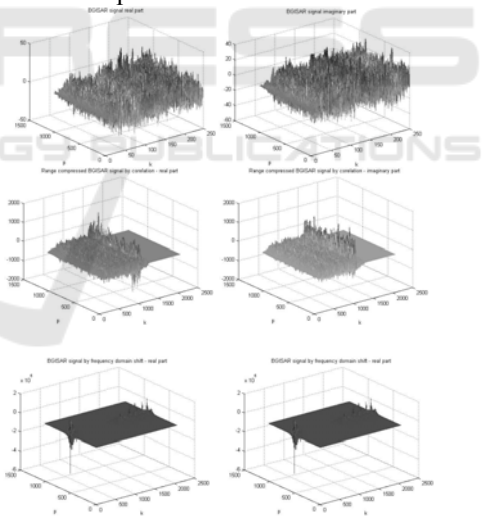

(a) (b)

Figure 14. BGISAR signal processing stages: real (a) and imaginary (b) parts, range compressed by correlation and azimuth compressed by Fourier transform.

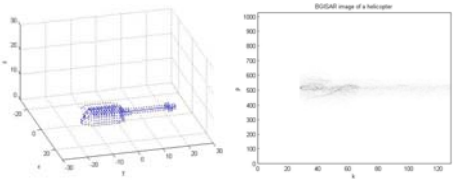

(a) (b)

Figure 15. Original image of helicopter (a) BGISAR image of helicopter (b)

# 3 BISTATIC FORWARD SCATTERING RADAR CONFIGURATIONS

## 3.1 Bistatic forward scattering radar processing

Bistatic forward scattering radar (BFSR) is a sub-class of bistatic radars, with a moving target and bistatic angle between transmitter-target-receiver close to $180^0$. The received signals are formed by diffraction of the emitted electromagnetic waves. The target can be considered as a secondary antenna which has the target's silhouette and with gain, defined by the target radar cross-section (RCS) which is independent from the target material. Such systems can be used for stealth targets detection.

### 3.1.1 BFSR Scenario

Consider a BFSR scheme using CW signals for situation awareness that includes a transmitter *T* and receiver *R* situated on the ground or see surface and a target with distances transmitter-target $R_T$ (*t*) and target-receiver $R_R$ (*t*), and bistatic angle θ(*t*) (Fig. 16). Targets (humans or vehicles) are moving across the transmitter-receiver baseline. A signature of a moving target is received at the background of clutter, noise and possibly interference.

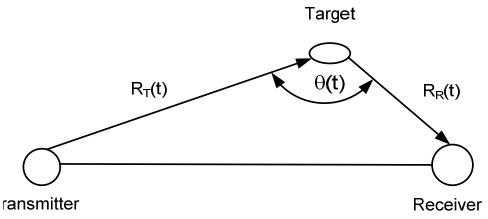


Figure 16: BFSR scenario.

The deterministic signal at the input of the receiving antenna is given by the sum of the direct transmitter-receiver (leakage) signal and the signal reflected from the target. The leakage signal is much stronger than the signal from the target which can be separated based on the Doppler signature induced by displacement of the target.

### 3.1.2 BFSR signal processing and parameter estimation

Signature processing includes signal compression and target resolution by maximization of signal-to-noise ratio (SNR) as the target signature could be buried under noise at longer baselines (Cheng Hu, 2008).

Let target's speed be a parameter estimated on the baseline. Assume that the signal is corrupted only by additive white Gaussian noise. SNR maximization is realized by correlating the received signal $S_T(t)$ with a reference function $S_0(t)$, complex conjugated of the target signature itself. The correlation process is described by the equation

$$S(\tau) = \int_{-\frac{T}{2}}^{\frac{T}{2}} S_T(t) S_0(t-\tau) dt \qquad (7)$$

where *T* is the coherent processing interval, $\tau$ is the correlation displacement.

This process is known as matched filtering, and referred to as optimal signal processing algorithm. If the reference function has a rectangular envelop, the signal processing is quasi optimal.

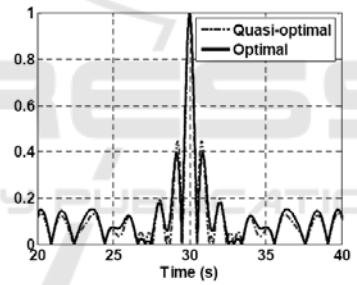


Figure 17: Signature compression by optimal and quasi optimal processing algorithms.

Compressed signatures for a single target obtain by optimal and quasi optimal processing algorithms are presented in Fig. 17.

## 3.2 BFSR radar cross section estimation

BFSR concept can be applied in monitoring and protecting coast lines and off shore territories. Using a chain of buoys, located on the sea surface and equipped with FSR transceivers, schematically shown in Fig. 18 (Liam Daniel, 2008).

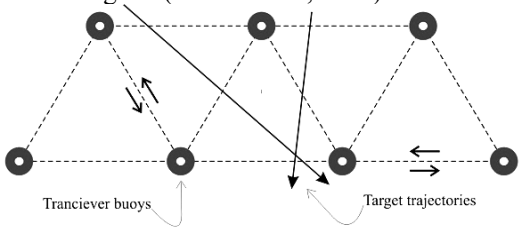

Figure 18: A chain of buoys, located on the sea surface and equipped with FSR transceivers

Objects crossing the baselines connecting adjacent transceiver buoys could be detected through analysis of their Doppler signature. Small targets with low radar reflectivity such as jet-skis, inflatable boats and swimmers could be detected.

BFSR RCS can be defined through optical approximation: BFSR RCS of a complex object is reduced to the radiation pattern of the silhouette shape of that object (black body approximation), and finding of the radiation pattern of this silhouette's uniformly (planar) illuminated complimentary plane aperture (Babinet's principle) (Fig. 19) (Daniel L., 2008).

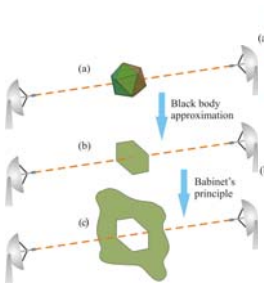


Figure 19

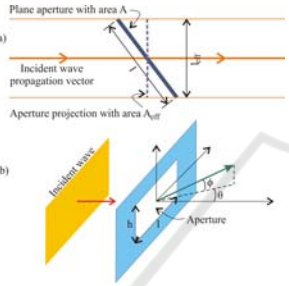


Figure: 20

Figure 19: Scatter from a complex object (a), reduced to scatter from a plane shape (b), further reduced to diffraction from an aperture (c).

Figure 20: Aperture projections in plane perpendicular to wave propagation vector and (b) angular definitions for analytic RCS (8).

In the direct forward scatter direction of incident wave propagation, the FS RCS $\sigma_{fs}(0°)$ is given by the following equation

$$\sigma_{FS}(0^0) = 4\pi \frac{(A_{eff})^2}{\lambda^2} \qquad (8)$$

$\lambda$ is the wavelength of the illuminating signal and $A_{eff}$ is the effective area of the aperture projected in the plane perpendicular to the incident wave propagation vector, shown in a top down view in Fig. 20(a). The calculation of RCS can be simplified even further by considering only purely rectangular shaped apertures. Thus the FS RCS in the analytical model approximation goes as,

$$\sigma(\theta,\phi) = \sigma_{FS}(0^0)\left[\frac{\sin\left(\frac{\pi l_{eff}}{\lambda}\sin\theta\right)}{\frac{\pi l_{eff}}{\lambda}\sin\theta}\right]\left[\frac{\sin\left(\frac{\pi h_{eff}}{\lambda}\sin\phi\right)}{\frac{\pi h_{eff}}{\lambda}\sin\phi}\right]$$

where $l_{eff}$ and $h_{eff}$ are the effective length and height of the aperture as defined like the effective area in (1) and also shown in Fig. 20(a). Angular definitions ($\theta$,$\phi$) are shown in Fig. 20(b).

## 3.2 BFSR automatic target classification network

The concept of a Forward Scattering Radar (FSR) wireless network has recently been presented for situational awareness in ground operations (Rashid N.E.A., 2008). Its primary objectives are the detection, parameter estimation (such as speed) and automatic target classification (ATC) of various ground targets (personnel, vehicles) entering or crossing its coverage area (Fig. 21).

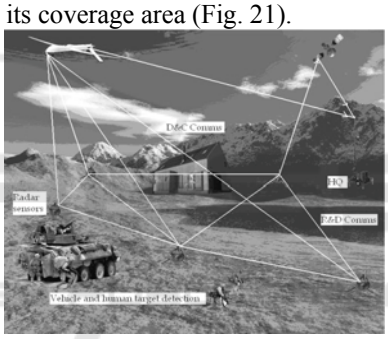


Figure 21: The concept of the FSR micro – sensors radar network (Sensors enlarged for visibility)

The system provides monitoring in remote or even inaccessible areas, and does not require manual installation of sensors. They could be spread into random positions directly on the ground from a remotely operated moving platform such as a UAV. The sensors in the wireless FSR network carry out:

- Communication to the central post (headquarter – HQ) using a wireless link through a UAV or a satellite for situational data transfer and receiving control commands (data and control – D&C).
- Neighboring nodes in the network create FSR channels and communicate to each other to transfer data and commands, if a direct link to a UAV or a satellite is impossible (radar and data lines – R&D.
- Sensors detect targets, roughly estimate target parameters and reject noise, clutter, interferences and reflections from unwanted targets (such as birds, animals).

### 3.3 Bistatic forward scattering inverse synthetic aperture radar

The geometry of BFISAR topology is presented in Fig. 22 (Lazarov A.). Consider stationary transmitter and receiver both located on sea surface and as a mariner target a ship all situated in a Cartesian coordinate system *Oxyz*. The target presented as an assembly of point scatterers is depicted in its own coordinate system *OXYZ*.

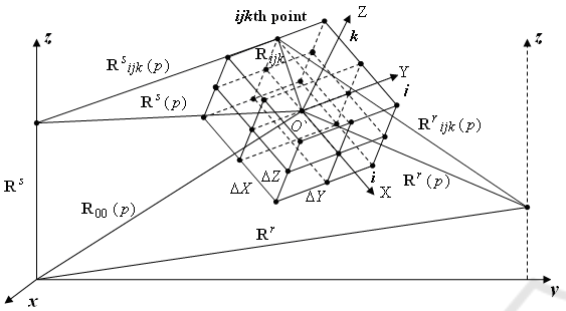


Figure 22: BFISAR Geometry

Assume linear frequency modulated (LFM) emitted signal. Then the deterministic component of BFISAR signal is superposition of signals reflected by all target's point scatterers, i.e.

$$\dot{S}(p,t) = \sum_{ijk} a_{ijk}\,\mathbf{rect}[T_{ijk}(t)]\mathbf{exp}\left\{-j\begin{bmatrix}\omega\left(t-t_{ijk}(p)\right)\\ +b\left(t-t_{ijk}(p)\right)^2\end{bmatrix}\right\}$$

where ω is angular frequency, *b* is the LFM rate, *p* is the number of emitted pulse.

Image reconstruction algorithm consists of

*Phase correction:* $\widetilde{S}(p,k) = \hat{S}(p,k).\exp\left[j\Phi(p,k)\right]$.

*Range compression by inverse Fourier transform over discrete range coordinate k*

$$\widetilde{S}(p,\hat{k}) = \frac{1}{K}\sum_{k=1}^{K}\widetilde{S}(p,k).\exp\left(j2\pi\frac{k\hat{k}}{K}\right),\ \hat{k}=\overline{1,K}$$

*Azimuth compression by inverse Fourier transform over discrete azimuth coordinate p*

$$a_{ijk}(\hat{p},\hat{k}) = \frac{1}{N}\sum_{p=1}^{N}\widetilde{S}(p,\hat{k}).\exp\left(j2\pi\frac{p\hat{p}}{N}\right),\ \hat{p}=\overline{1,N}\ .$$

#### 3.3.1 BFISAR numerical experiment

Assume a target (ship on sea) is moving rectilinearly in *Oxyz*. Transmitter coordinates: $x^s = -250$ m; $y^s = 0$ m; $z^s = 15$ m. Receiver coordinates: $x^r = 300$ m; $y^r = 0$ m; $z^r = 12$ m. Target parameters: velocity $V = 14$ m/s; LFM pulse's parameters: wavelength $\lambda = 3.10^{-2}$ m, pulse repetition period $T_p = 3{,}2.10^{-3}$ s, pulse width $T = 9.10^{-6}$ s, number of LFM samples $K = 256$, carrier frequency $f = 10^{10}$ Hz, sampling period $\Delta T = T/K = 1.56.10^{-8}$ s, signal bandwidth $\Delta F = 2.10^8$ Hz, LFM rate $b = 1{,}39.10^{14}$, number of transmitted pulses $N = 256$. Target geometry is depicted in a 3-D regular grid with cell's dimensions $\Delta X = \Delta Y = \Delta Z = 0.5$ m.

BFISAR signal, BFISAR range compressed signal and BFISAR azimuth compressed signal for $x_{00}(0) = 25$ m; $y_{00}(0) = 150$ m; $z_{00}(0) = 0$ m are presented in Figs. 23, 24 and 25.

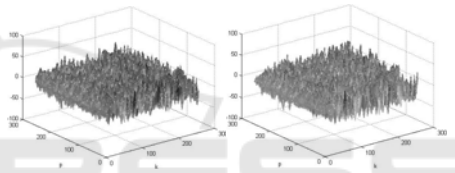

Figure 23: BFISAR signal: real (a) and (b) imaginary part.

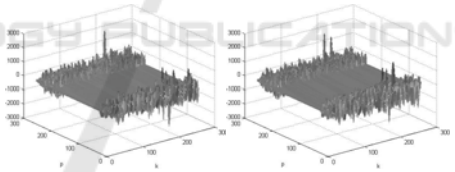

Figure 24: BFISAR range compresed signal: real (a) and (b) imaginary part.

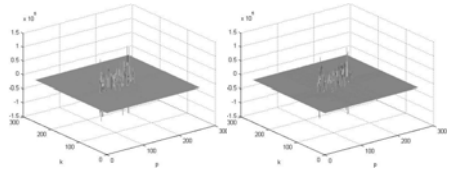

Figure 25: BFISAR azimuth compressed and shifted signal: real (a) and (b) imaginary part.

BFISAR images of the ship target at a position (*a*): $x_{00}(0) = 25$ m, $y_{00}(0) = 150$ m, $z_{00}(0) = 0$ m, and position (*b*): $x_{00}(0) = 25$ m, $y_{00}(0) = 50$ m, $z_{00}(0) = 0$ m, are presented in Fig. 26.

SCITEPRESS SCIENCE AND TECHNOLOGY PUBLICATIONS

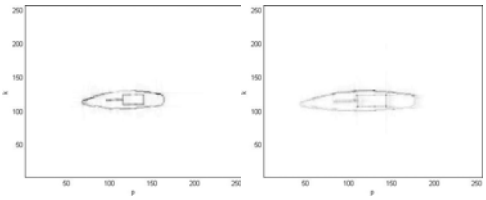

(*a*) (*b*)

Figure 26: BFISAR images: $y_{00}$=150 m (*a*), $y_{00}$ =50 m (*b*).

# 4 CONCLUSION

In this work bistatic radar concept and its realization are thoroughly discussed. Different BSAR configurations are analyzed. BSAR geometry and radar equation are defined. Detailed description of BSAR implementation with uncooperative satellite transmitter is presented. Special attention is given to BFSAR and BFISAR. Optimal and quasi optimal signal processing in target parameter estimation is defined. Optical approximation approach including black body approximation and Babinet's principle is applied in definition of forward scattering radar cross section. Analytical signal model of BGISAR and BFISAR and corresponding image reconstruction algorithms are presented. Results of numerical experiments are discussed. It is proven that bistatic synthetic aperture radar and even its forward scattering concept is applicable in target imaging with acceptable resolution.

# ACKNOWLEDGEMENTS

This work is supported by NATO project ESP.EAP.CLG.983876 and MEYS, Bulgarian Science Fund the project DTK 02/28.2009, DDVU 02/50/2010.

# REFERENCES

Moccia A., Rufmo, G., D'Errico M., Alberti, G., et. Al. 2002. BISSAT: A bistatic SAR for Earth observation In *IEEE International Geoscience and Remote Sensing Symposium (IGARSS'02)*, Vol. 5, June 24-28, pp. 2628-2630.

Cherniakov M. 2002. Space-surface bistatic synthetic aperture radar Prospective and problems, In *International Conference of Radar*, Edinburgh, UK, pp. 22-26.

Ender J. H. G., I. and A. R. Brenner 2004. New aspects of bistatic SAR: Processing and experiments. In *2004 Proceedings of International Geoscience and Remote Sensing Symposium (IGARSS)*, vol. 3, Anchorage, AK, Sept. 20—24, 2004, pp. 1758—1762.

Whitewood A., Muller B., Griffiths H., and Baker, C. 2003. Bistatic SAR with application to moving target detection. In *International Conference RADAR-2003*, Adelaide, Australia.

D'Aria D., A. M. Guarnieri, and F. Rocca, Focusing bistatic synthetic aperture radar using dip move out, *IEEE Transactions on Geoscience and Remote Sensing*, 42, no. 7, 2004, pp. 1362—1376.

Martorella M., Palmer J., Homer J., Littleton Br., and Longstaff D. 2007. On bistatic inverse synthetic aperture Radar, *IEEE, Transaction on Aerospace Electronic System*, vol. 43, no. 3, pp. 1125-1134.

Cherniakov M., Plakidis E., Antoniou M., Zuo R. 2009. Passive Space-Surface Bistatic SAR for Local Area Monitoring: Primary Feasibility Study. *In 6th European Radar Conference,* 30 Sept. - 2 Oct. 2009, Rome, Italy, pp 89-92.

Whitewood A.P., Baker C.J., Griffiths H.D. 2007. Bistatic radar using a spaceborne illuminator. In *IEE international radar conference*, Edinburgh, October 2007.

Antoniou M., Saini R., Cherniakov M. 2007. Results of a Space-Surface bistatic SAR image formation algorithm, *IEEE Trans. GRS*, vol. 45, no. 11, pp. 3359-3371.

He X., Cherniakov M., Zeng T. 2005. Signal detectability in SS-BSAR with GNSS non-cooperative transmitter. In *IEE Radar, Sonar and Navigation*, vol. 152, no. 3, pp. 124-132, June, 2005.

Antoniou M., Zuo R., Plakidis E., Cherniakov M. 2009. Motion compensation algorithm for passive Space-Surface Bistatic SAR, In *Int. Radar Conf*., Bordeaux, France, October 2009.

Willis N.J., Griffiths H.D. 2007. *Advances in bistatic radar*, SciTech Publishing Inc.

Zuo R., Saini R., Cherniakov M. 2007. Non-cooperative transmitter selections for Space-Surface Bistatic SAR. *Anual Defence Technology Centre (DTC) Conference*, Edinburgh.

Saini R., Zuo R., Cherniakov M. 2009. Signal synchronization in SS-BSAR based on GLONASS satellite emission, DECE, University of Birmingham.

Cherniakov M., Plakidis E., Antoniou M., Zuo R. 2009. Passive Space-Surface Bistatic SAR for Local Area, Monitoring: Primary Feasibility Study, In *2009 EuMA,* 30 September - 2 October 2009, Rome, Italy

Daniel L., Gashinova M., Cherniakov M.. 2008. Maritime Target Cross Section Estimation for an Ultra-Wideband Forward Scatter Radar Network, In *2008 EuMA, Amsterdam*, pp. 316-319.

Lazarov A., Kabakchiev Ch., Rohling H., Kostadinov T. 2011. Bistatic Generalized ISAR Concept with GPS Waveform. In *IRS, Leipzig*, pp. 849-854.

Lazarov A., Kabakchiev Ch., Cherniakov M., Gashinova M., Kostadinov T. 2011. Ultra Wideband Bistatic Forward Scattering Inverse Synthetic Aperture Radar Imaging. In *2011 IRS, Leipzig*, pp. 91-96.

## BRIEF BIOGRAPHY

Andon Dimitrov Lazarov received MS degree in Electronics Engineering from Sent Petersburg Electro-technical State University, Russia in 1972, and Ph. D. degree in Electrical Engineering from Air-Defense Military Academy, Minsk, Belarus in 1978, and Doctor of Sciences degree from Artillery and Air-Defense University, Bulgaria. From 2000 to 2002 he is a Professor at the Air Defence Department with Artillery and Air-Defense University. From 2002 he is a Professor with Bourgas Free University. He teaches Discrete Mathematics, Coding theory, Antennas and Propagation, Digital Signal Processing, Mobil Communications. His field of interest includes SAR, ISAR and InSAR modeling and signal processing techniques. He has authored above 150 research journal and conference papers. He is a secretary of Commission F of URSI Committee – Bulgaria, and a member of the IEEE, AES-USA, and in reviewer and editorial boards of IET - Canada, PIER & JEMWA – USA, Journal of radar technology, Beijing, China. EURASIP Journal on advances in signal processing - USA.

SCITEPRESS
SCIENCE AND TECHNOLOGY PUBLICATIONS